JOURNAL OF THERMOPHYSICS AND HEAT TRANSFER
Vol. 25, No. 3, July–September 2011

Temperature Measurements of Air Plasma Flow Using Optical Emission Spectroscopy

Alessio Cipullo*
Second University of Naples, 81031 Aversa, Italy
Federico De Filippis†
Italian Aerospace Research Center (CIRA), 81043 Capua, Italy
and
Luigi Zeni‡
Second University of Naples, 81031 Aversa, Italy

DOI: 10.2514/1.49305

The rotational temperature of the freestream flow generated by the Scirocco arcjet plasma wind-tunnel facility of the Italian Aerospace Research Center (CIRA) is measured by means of optical emission spectroscopy. The gas mixture used to perform the atmospheric reentry simulation tests is air, and the optical spectrum emitted 17 cm away from the exit section of the nozzle has been investigated over the 220–310 nm wavelength range. The optical setup is based on a 1200-grooves/mm monochromator and a 1024 × 256 charge-coupled device camera, and the spectrum has been calibrated using a combined deuterium–halogen radiation source. The rotational temperature is determined by comparing the experimental spectra with those obtained by the spectral simulation software LIFBASE 2.0. A pattern-matching algorithm is used. Attention is mainly focused on the NO emission bands, and partial agreement between experimental results and numerical predictions is achieved for six test campaigns conducted in the arcjet facility. Finally, an error analysis has been performed to assess the error bands of the measures.

Nomenclature

A	=	emission coefficient
I	=	emission intensity
k	=	Boltzman constant, 1.3806×10^{-23} J/K
k_p	=	predissociation rate
N	=	number density
Q_{elec}	=	electronic partition function
Q_{rot}	=	rotational partition function
Q_{vib}	=	vibrational partition function
T_{rot}	=	rotational temperature
T_{vib}	=	vibrational temperature
ε_{tot}	=	total relative error

Subscripts

v', J'	=	higher vibrational and rotational levels
v'', J''	=	lower vibrational and rotational levels

I. Introduction

THE simulation of thermal and mechanical loads encountered by a spacecraft during the atmospheric reentry is one of the most challenging research areas in the aerospace field. The knowledge of the involved physical and chemical processes is extremely important in a number of applications, e.g., design and validation of thermal protection systems. The development of investigation techniques for a detailed and accurate flow characterization is, therefore, a necessary step. It is well known that the harsh conditions during tests require nonintrusive measurement techniques; therefore, conventional and nonconventional spectroscopic investigations of spontaneous or induced radiation are extremely useful to measure temperature, pressure, velocity, and concentration of the chemical species in equilibrium and nonequilibrium conditions. Valuable examples of spectroscopy applications can be found in Park et al. [1] and in De Filippis et al. [2]. During the last few years, considerable efforts have been put to measure the rotational temperature of the high-enthalpy plasma flow produced by the Scirocco arcjet facility at the Italian Aerospace Research Center (CIRA). Among different techniques, optical emission spectroscopy (OES) has been selected. The main advantages of the OES are nonintrusivity, high sensitivity, and the possibility to access detailed information about chemistry and physics of the plasma [3–6]. In the present work, the attention has been focused on the A–X vibrational bands emitted by the NO molecules, located in the near-UV region. This work represents the further development of the work carried out by De Filippis et al. [2], where the OES technique has been applied to identify the main contributors of the Scirocco plasma jet radiation. Determining the rotational temperature by means of the minimization of the relative error function between experimental and predicted spectra represents the main goal of the present study.

II. Theoretical Background

The initial composition of the air plasma under investigation reads 76.6% N_2 and 26.4% O_2, plus a small concentration of H and Ar. The gas mixture is injected in the arc column, and it is brought to high temperatures and high enthalpy by the effect of the electric arc. The energy levels of the species in the mixture are excited, and chemical reactions such as dissociation, ionization, and recombination take place, forming a mixture for which the most important species are N, O, N_2, O_2, NO, and H. Successively, in passing through the converging–diverging nozzle, the strong expansion induces part of the thermal energy to transform into kinetic energy. Because of the high flow velocities and different relaxation times [4–6] of the involved reactions, the process gas has to be considered in a

Received 10 February 2010; revision received 8 February 2011; accepted for publication 9 February 2011.

*Ph.D. Student, Department of Information Engineering, via Roma, 29; alex.cipullo@virgilio.it.
†Head, Diagnostics and Monitoring Techniques, via Maiorise; f.defilippis@cira.it.
‡Professor, Department of Information Engineering, via Roma, 29; zeni@unina.it.

thermochemical nonequilibrium state. According to simulations carried out for the conical nozzle model [7–9], the rotational temperature becomes of the same order as the translational one at the exit section; that is, these two temperatures can be assumed to be in equilibrium. In contrast, large differences among rotational, vibrational, and electronic temperatures have been found. This is the reason why the rotational temperature is extremely important for the freestream plasma flow characterization and, due to the particular physical properties of the plasma, nonintrusive measurement methods, such as emission spectroscopy, are extremely useful.

The spontaneous emission spectrum is a collection of spectral lines and bands rising from transitions between higher and lower energy levels. Transition mechanisms are rather complex, so only in simple cases (e.g., for the NO) an accurate model has been derived [10]. Among chemical species, NO has been selected because of its significant emission rate. In particular, the molecular vibrational band systems analyzed in this work are in the wavelength range 220–310 nm, and they correspond to the bands from γ-(0, 0) to γ-(0, 6), related to the NO electronic transition from the third level $A^2\Sigma$ to the ground level $X^2\Pi$. However, only the first six bands [from (0, 1) to (0, 6)] have been taken into account for elaborations. The low signal-to-noise ratio (SNR) below 230 nm, due to significant air absorption along the optical path, prevents accurate analysis.

In the reference model [3], the wavelength positions of spectral lines are calculated from expressions derived from the corresponding Hamiltonians (in particular, this is the N formalism, known as Brown's Hamiltonians [11]). An emission intensity value is associated to each one of the wavelength positions (they correspond to transitions between the higher vibrational and rotational levels v' and J' and the lower ones v'' and J''):

$$I_{v''J''}^{v'J'} \propto N_{v'J'} \frac{A_{v''J''}^{v'J'}}{\sum_{v''J''} A_{v''J''}^{v'J'} + Kp_{v'J'}} (1 - e^{-(t/\tau)}) \tag{1}$$

$A_{v''J''}^{v'J'}$ denotes the emission coefficients [s^{-1}] between the higher levels v', J' and the lower levels v'', J''; $Kp_{v'J'}$ is the predissociation rate; and τ[s] is the effective lifetime.

$N_{v'J'}$ is the number density of the excited state, and it depends on both rotational and vibrational temperatures, T_{rot} and T_{vib}:

$$\begin{aligned} N_{v'J'} &= N_0 \cdot f_B(v', J') \\ &= N_0 \cdot \frac{e^{-\{[E(v')]/(kT_{\text{vib}})\}} \cdot (2J' + 1) \cdot e^{-\{[E(J')]/(kT_{\text{rot}})\}}}{Q_{\text{vib}} \cdot Q_{\text{rot}} \cdot Q_{\text{elec}}} \end{aligned} \tag{2}$$

N_0 denotes the number density of the excited state, and $f_B(v', J')$ is the Boltzman fraction. Q_{vib} and Q_{rot} are the vibrational and rotational partition functions calculated numerically [3] (the classical multi-Boltzmann distribution is used), and Q_{elec} is the electronic partition function, and it is assumed to be equal to the electronic degeneracy $g_e = (2 - \delta_{O,\Lambda})(2S + 1)$. The equation $2S + 1$ is the spin multiplicity factor, and $\delta_{O,\Lambda} = 1$ for Σ states and 0 for the others.

The reference model takes into account the Doppler shift and the instrumental, Doppler, and pressure broadenings. Further details can be found in Luque and Crosley [3].

According to Park [12], in a typical hypersonic flight environment, pressure broadening is of the same order as the Doppler one, while natural broadening (predissociation broadening) may be neglected.

III. Experimental Setup

The Scirocco hypersonic plasma wind tunnel is a large-scale arcjet facility, and it has been used to emulate reentry conditions in Earth atmosphere since its official birth in 2001 (Fig. 1). A dc power supply delivers a maximum electrical power of 70 MW to the 5.5-m-long segmented constricted arc heater. The compressed air mixture (1–16.7 bar) is therefore energized, and a high-enthalpy (2.5–45 MJ/kg) high-temperature (up to 10,000 K) flow enters a converging–diverging conical nozzle. Seven different configurations are possible for the diverging part of the conical nozzle, with an exit diameter ranging between 0.187 and 1.950 m. The maximum achievable Mach number is 7. An 80 MW pumping system allows for a vacuum pressure of 0.2 mbar in the test chamber and, finally, a 50-m-long diffuser slows down the flow to the subsonic regime and releases it into the atmosphere. The arc heater, the conical nozzle, the diffuser, and the electrical apparatus are cooled by means of high-pressure deionized water. Detailed descriptions of the facility can be found in the literature [13–19].

The setup for spectral measurements is sketched in Fig. 2. The radiation was collected by a Nikon UV-Nikkor objective. It has a focal length $f = 105$ mm and a maximum aperture of $f/4.5$. A mercury radiation source was used to calibrate the acquired raw spectra and to evaluate the instrumental resolution. Moreover, the particular lens arrangement inside the UV-Nikkor minimizes the chromatic aberration and distortion [20]. The line of sight is not perpendicular to the plasma flow centerline, so a transversal component arises; however, this is considered negligible because of an overangle less than 1°. The monochromator is a Horiba Jobin Yvon HR460. It has a plane holographic blazed 1200-grooves/mm grating with a ± 0.15 nm wavelength position accuracy and a total scanning range of 200–1300 nm with a slew rate of 45 nm/s. The instrumental

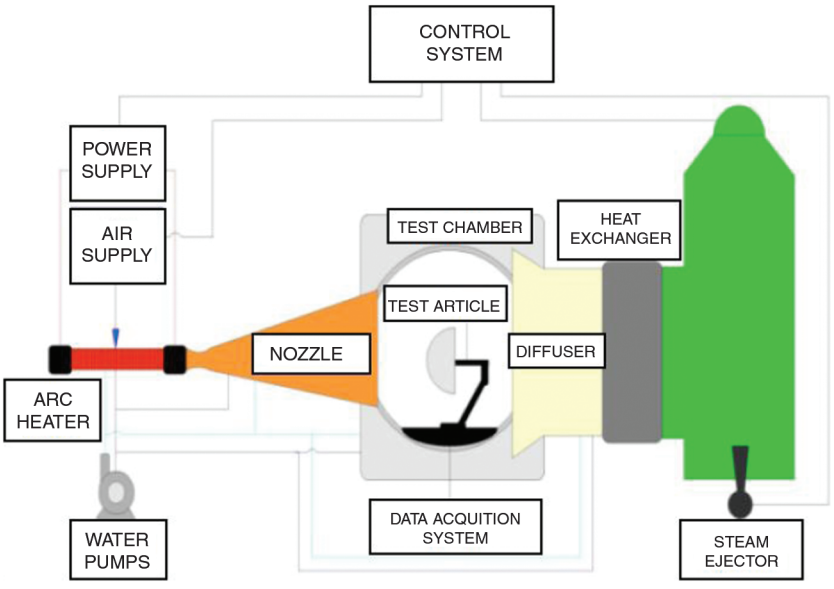

Fig. 1 Scirocco facility scheme.

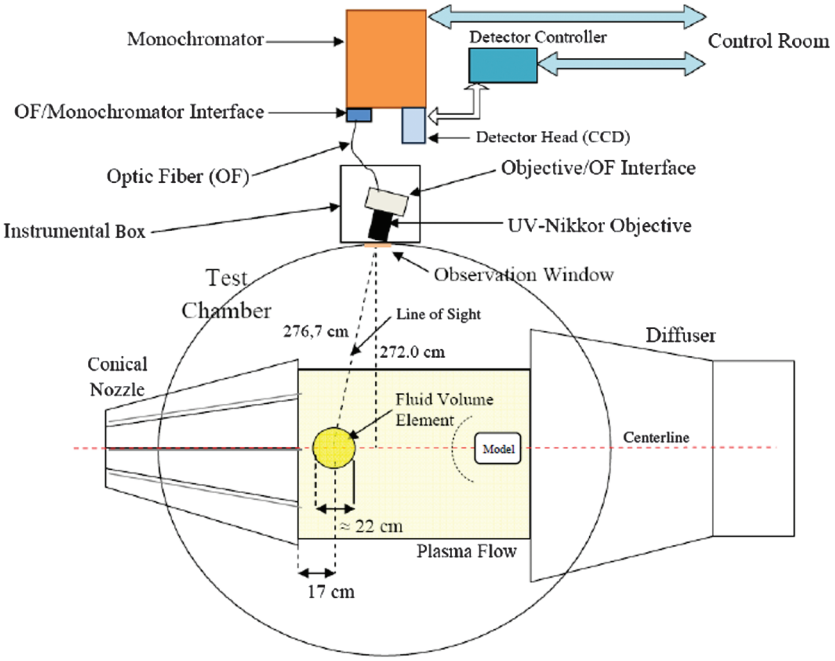

Fig. 2 Optical system arrangement–top view of the test chamber (elements are not in scale).

resolution was deduced experimentally by comparing atomic lines of the experimental and theoretical spectra of a mercury lamp: a value of 0.7 nm (full-width half-maximum) was obtained. Emission spectra are then imaged by the Horiba Jobin Yvon Symphony charge-coupled device (CCD) camera (1024 × 256 pixels, each pixel having a 26 × 26 μm size). It has a four-stage thermoelectric cooling system (based on Peltier cells) to work at about 200 K (to ensure a maximum dark current of 0.008e-/pixels/s). The CCD camera is controlled by a detector controller, and there is a remote control for the whole optical measurement system in the control room of the facility.

Intensity calibrations were performed at atmospheric pressure by a combined deuterium–halogen lamp (Avantes AvaLight-DHc). The measured spectrum in the range of interest (220–310 nm) was divided by the theoretical lamp spectrum (Fig. 3) to obtain the absolute response curve of the optical setup, The percentage response curve is reported in Fig. 4. The distance from the centerline to the objective is about 277 cm, and the lamp is a low power source; hence, it was decided to place the lamp as close as possible to the observation window to account for the response of the observation window, objective, optical fiber, grating, and CCD detector. Since the calibration has been performed in relative units, it can be considered reliable even though the actual optical path length is not reproduced. Calibrated spectra were computed by simply dividing the raw acquired spectra by the absolute response curve. The calibration procedure was repeated several times to assess both short-term (5 min) and long-term (one day) repeatability. In the first case, the difference between the integrals of the emitted spectra was 5%, and in the second case, it was 7%. As it is possible to observe from Fig. 3, discontinuities on the experimental spectrum of the lamp are present in correspondence of about 245 and 292 nm: they are given by the grating and CCD response. They were not corrected, so as to get rid of their effect on the calibrated spectrum.

The temporal stability of the plasma jet was assessed by monitoring the nozzle exit pressure, the total pressure in the column, the supplied voltage, and the current. In particular, the fast Fourier transform of the quantities was performed, and no significant frequency components were observed except the dc. Regarding the spatial uniformity of the jet, a cooled probe is normally used to span the radius of the jet and to measure stagnation pressure and heat flux. Both quantities are uniform along the radius, and they have a step decay in correspondence of the boundary layer (see Caristia et al. [21] and references therein). Therefore, it is assumed that the plasma jet is approximated by a uniform and homogeneous column. That is the reason why the rebuilding of the local emission through a deconvolution technique (such as Abel inversion) is avoided, and only the line-of-sight emission is considered.

IV. Data Analysis Procedure

The main goal of this work was to measure the rotational temperature of the freestream plasma flow by comparing experimental spectra to those simulated by means of LIFBASE 2.0 [3]. To this end,

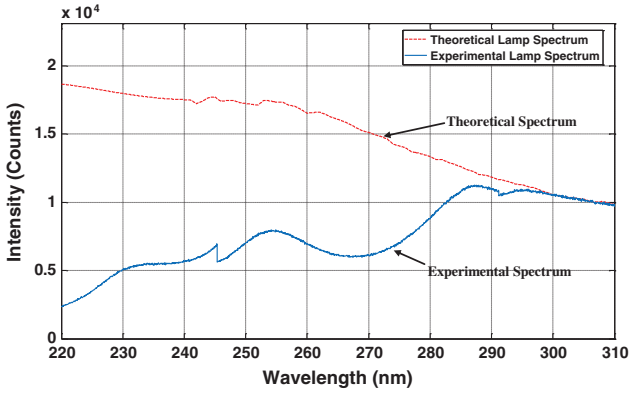

Fig. 3 Theoretical and experimental lamp spectra for intensity spectral calibration in the range 220–310 nm.

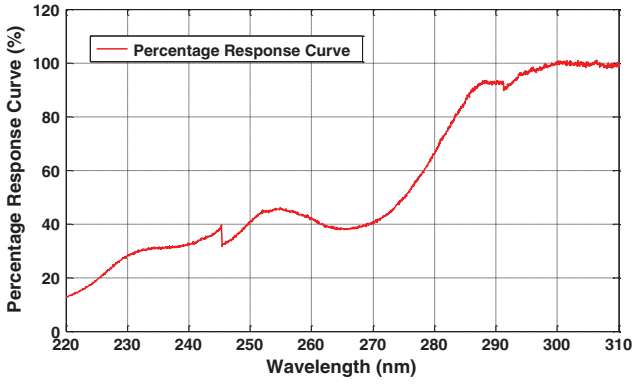

Fig. 4 Percentage response curve of measurement chain for intensity calibration.

Table 1 Parameters for spectral simulation

Parameter	Description	Value	Units
λ_{START}	Start wavelength	220	nm
λ_{END}	End wavelength	310	nm
T_{rot}	NO rotational temperature	variable	K
T_{vib}	NO vibrational temperature	867	K
P	Plasma flow pressure	2	mbar
D	First collisional broadening parameter	400	——
L	Second collisional broadening parameter	1	——
$\Delta\upsilon$	Instrumental resolution	0.7	nm
υ_m	Plasma speed (Doppler shift)	4	km/s

a database has been created and filled with 201 simulated spectra. Each spectrum is characterized by a different rotational temperature belonging to the range 200–2000 K (with a step of 10 K), which is the typical rotational temperature range of interest for the considered test cases. All the other parameters are fixed for each test case. An example is reported in Table 1 for test 1 (see Tables 2–4).

The vibrational temperature T_{vib} has been obtained by the simulation code H2NS developed at CIRA (see De Filippis et al. [22] and references therein), the plasma flow pressure P has been determined experimentally, and the plasma speed υ_m has been derived from historical data, while D and L have been chosen to obtain a collisional broadening of the same order of the Doppler one (as already mentioned in Sec. II). The simulated NO emission spectrum between 220 and 310 nm is dominated by seven γ vibrational bands, from $(0,0)$ to $(0,6)$, related to the $X^2\Pi - A^2\Sigma$ electronic transition. Simulated spectra obtained by LIFBASE clearly show that, in the temperature range of interest, when the rotational temperature grows, the probability of transitions with higher energy gaps increases. As a consequence, lower wavelength emission lines can be observed and the change in the band shape becomes evident (Fig. 5). This well-known mechanism is the basis of the measurement technique implemented in this work.

The quantitative comparison between experimental and simulated spectra is performed for each single vibrational band [from $(0,1)$ to $(0,6)$] using a pattern-matching algorithm: the simulated band that minimizes the total relative error (in absolute value) represents the best approximation for the experimental rotational temperature. Total relative error function is defined in Eq. (3):

$$\varepsilon_{TOT} = \frac{1}{\Delta\lambda}\sum_{k=1}^{n}\varepsilon_k = \frac{1}{\Delta\lambda}\sum_{k=1}^{n}\left|\frac{S_k^{EXP} - S_k^{REF}}{S_k^{REF}}\right| \tag{3}$$

where ε_{TOT} is the normalized total relative error, ε_k is the kth relative error, S_k^{EXP} is the kth sample of the experimental vibrational band, S_k^{REF} is the kth sample of the simulated vibrational band, and n is the total number of samples. Finally, each total relative error is normalized by the bandwidth of interest $\Delta\lambda$ to ensure a consistent comparison among results. The choice of the relative error is related to the greater importance of the shape of the bands close to their bases. In fact, rotational temperature mainly influences the left tail of the band (see Fig. 5). The normalization by S_k^{EXP} allows one to give more emphasis to this part with respect to the top of the band.

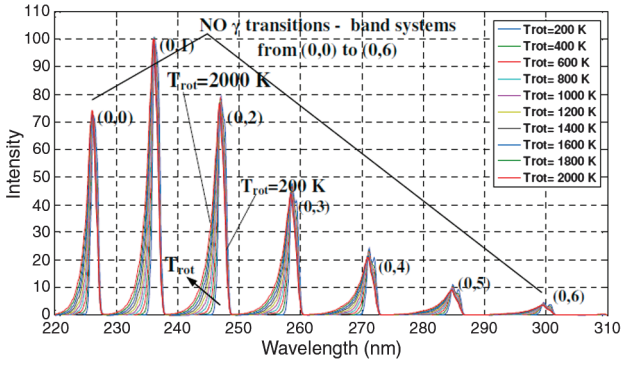

Fig. 5 NO simulated emission spectra between 220 and 310 nm.

Table 2 Vibrational bands: analysis ranges

Vibrational band	Range, nm
(0, 1)	235.0–237.5
(0, 2)	246.0–248.5
(0, 3)	257.5–260.0
(0, 4)	270.0–272.5
(0, 5)	283.5–286.2
(0, 6)	298.5–301.0

An independent computation for each one of the six bands has the advantage of a more flexible choice about the analysis ranges (they are reported in Table 2), together with the possibility of a simple statistical analysis. Both simulated and experimental spectra have been normalized in amplitude in order to perform a proficient comparison between them.

Figure 6 presents the application of the pattern-matching algorithm to the γ-(0, 1) band for test 1 (see Tables 2–4) conducted in the Scirocco facility. Results gave a best-matched simulated band characterized by a 410 K rotational temperature.

It is highly significant to put in evidence that the relative error minimization passes through the minimization of the error function for each band. Besides this, as it is possible to see from Fig. 7 for test 1 (analogous results have been found for the other five tests), all the error functions [Eq. (3)] have a single well-defined absolute minimum point. A direct identification of the rotational temperature associated to the minimum total relative error is then always possible.

V. Results and Discussion

The algorithm was applied to six tests (labeled with a progressive number from 1 to 6), and the experimental results were compared with computational fluid dynamics (CFD) predictions [22]. Figures 8 and 9 present the bands from γ-(0, 2) to γ-(0, 6) for test 1. Figure 10 is the comparison over the whole range of interest (220–310 nm).

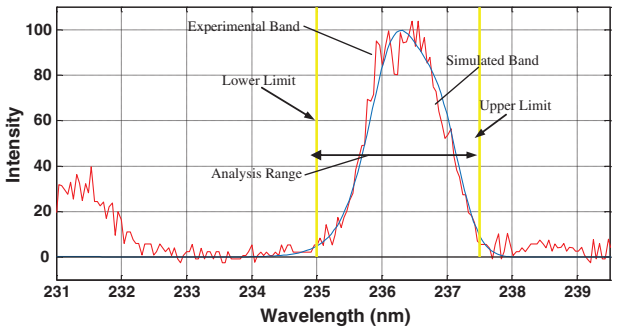

Fig. 6 Minimization algorithm result of vibrational band (0, 1): test 1.

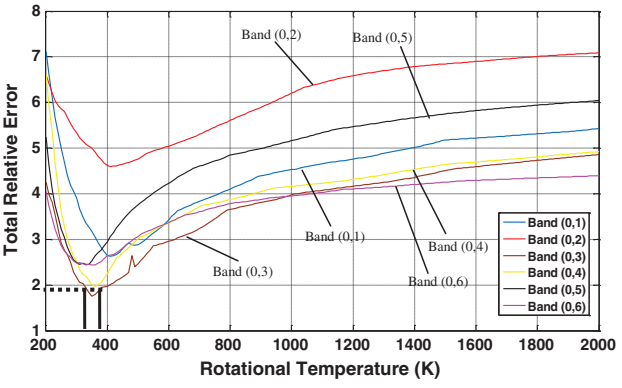

Fig. 7 Error functions for bands from (0, 1) to (0, 6): test 1.

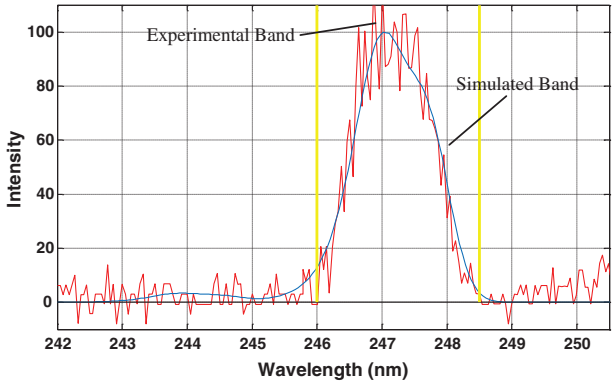

Fig. 8 Minimization result for vibrational band (0, 2): test 1.

Table 3 Experimental results: test 1

Vibrational bands	T_{rot}, K
(0, 1)	410 ± 45
(0, 2)	410 ± 35
(0, 3)	350 ± 15
(0, 4)	360 ± 21
(0, 5)	340 ± 17
(0, 6)	350 ± 25

Test 1 was performed with a nozzle-exit section diameter of 1950 mm, a total enthalpy of 13.1 MJ/kg, a nominal static temperature of 322 K, and a NO vibrational temperature coming from CFD predictions of 867 K. The summary of the experimental results for each band is reported in Table 3. The error analysis was performed

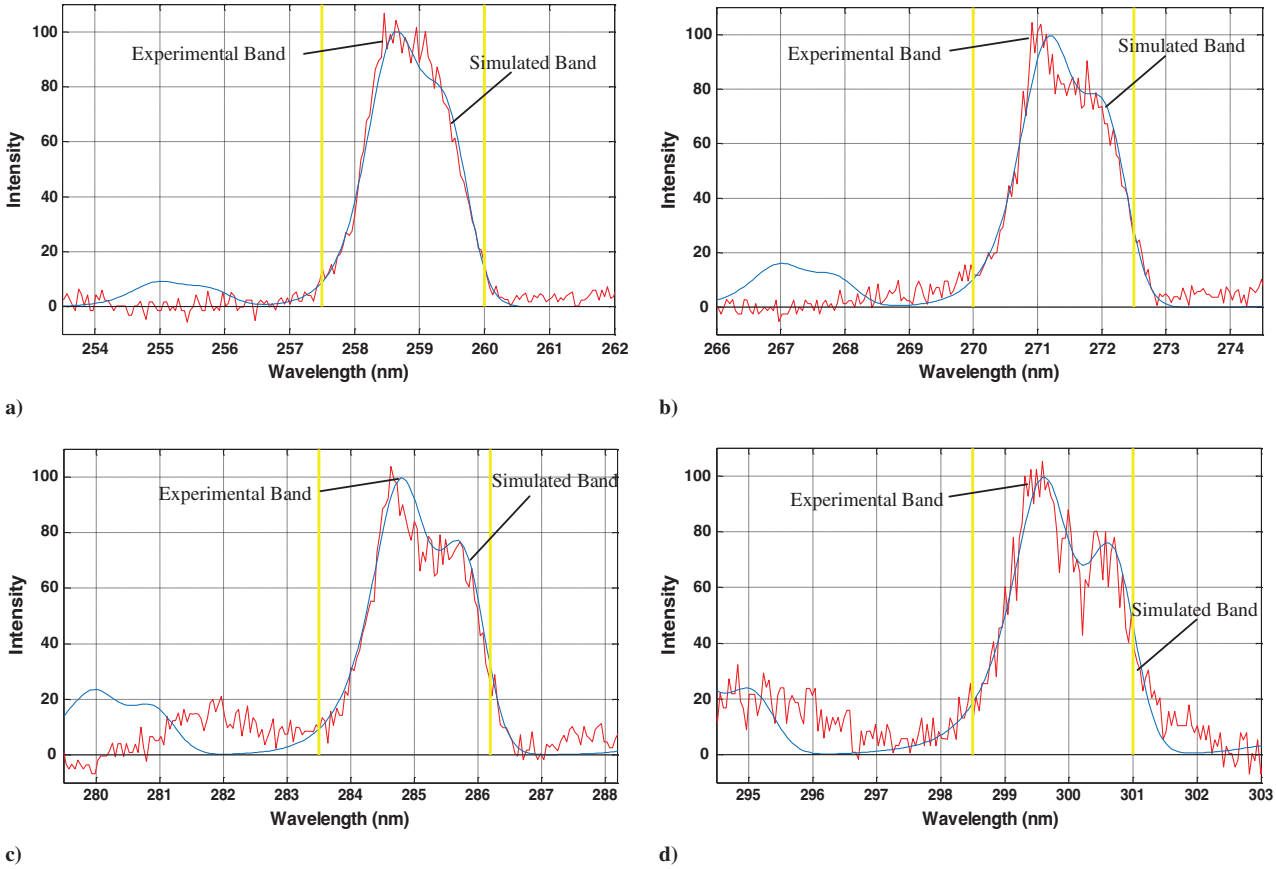

Fig. 9 Minimization results for vibrational band a) (0, 3), b) (0, 4), c) (0, 5), and d) (0, 6); test 1.

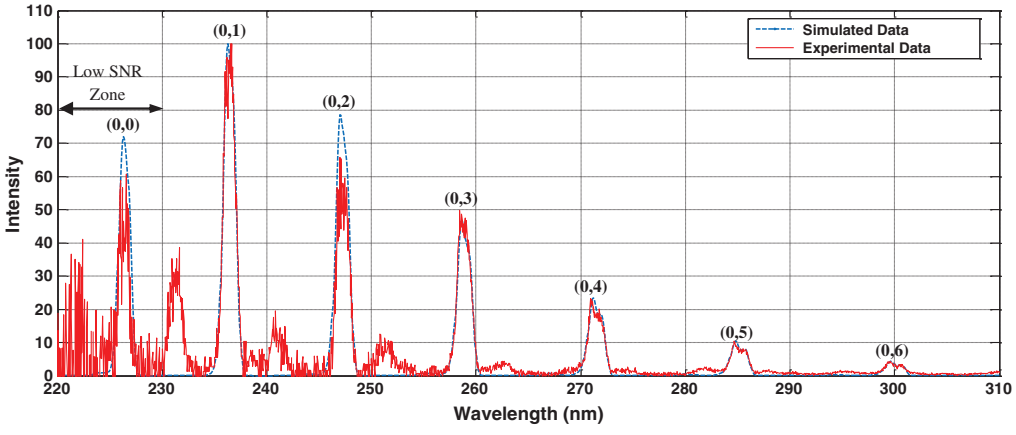

Fig. 10 Comparison between experimental and simulated emission spectra: test 1.

Table 4 Comparison between CFD predictions and experimental results for six tests performed in the Scirocco facility

Test	Nozzle-exit section diameter, mm	Total enthalpy–H_0, MJ/kg	CFD T_{rot} previsions, K	Experimental T_{rot}, K
1	1950 (F config.)	13.1	322	350 ± 18
2	1950 (F config.)	15.4	362	363 ± 35
3	1950 (F config.)	15.9	372	366 ± 42
4	1150 (D config.)	11.2	602	897 ± 67
5	900 (C config.)	8.8	640	690 ± 41
6	900 (C config.)	12.2	878	1020 ± 101

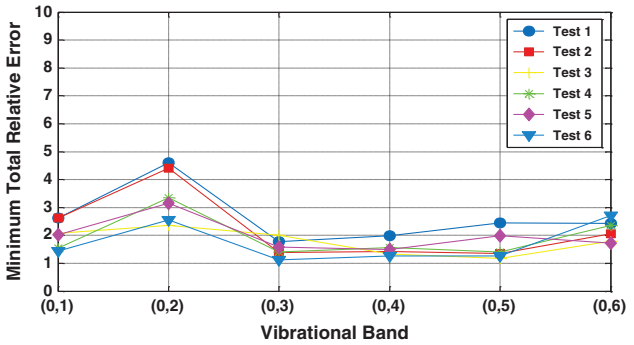

Fig. 11 Minimum total relative error for the six tests performed.

by applying the propagation of the error on Eq. (3), considering the experimental spectrum as the only source of error. A total error of 15% was estimated on the absolute intensity (including calibration error and repeatability, monochromator and CCD responses, and background noise). The resulting error ($\Delta\varepsilon_{TOT}$) was then projected on the ε_{TOT} profiles of Fig. 7, and the error on the rotational temperature was obtained [an example is reported in Fig. 7 for band (0,3)].

The average value of the experimental temperatures represents the final measure of the temperature, and the standard deviation is an indication of the dispersion, so $T_{rot} = 350 \pm 18$ K. Notice that the temperatures obtained from the bands are all in agreement within the error bands. It has been decided to exclude from the average the first and the second bands, because results are highly affected by noise. Averaging was performed without weighting temperature values; relative errors are, in fact, all of the same order (see Fig. 11).

Final results for the six tests performed are summarized in Table 4. There is acceptable agreement between CFD data coming from the simulations of the Scirocco internal flow hypersonic behavior and experimental results when the F configuration (1950 mm jet diameter) is used (tests from 1 to 3) for the conical nozzle. Measurement errors are of the order of 10%. In contrast, there is only a partial agreement when C (950 mm diameter) or D (1150 mm diameter) configurations are used (tests 4 to 6); however, the error on the temperature is around 10% as well.

VI. Conclusions

The thermal properties of the plasma flow generated by the Scirocco arc-heated high-enthalpy facility have been investigated using OES. A simple pattern-matching method has been proposed as the first step to evaluate the rotational temperature of the freestream plasma jet. The experimental NO γ-$(0,1)$ to γ-$(0,6)$ vibrational bands have been compared with those simulated using the software LIFBASE 2.0. Furthermore, assuming equilibrium between rotational and translational modes, the measured rotational temperature gave a highly significant direct indication of the plasma flow temperature.

The experimental results obtained for six test campaigns have shown agreement with CFD simulations for the F configuration (diameter of the nozzle of 1950 mm), with a maximum measurement error of about 10% with respect to the CFD result. In contrast, only a partial agreement for the C (diameter of 900 mm) and D (diameter of 1150 mm) configurations has been achieved, with a measurement error of 10% as well. The investigation of additional electronic bands and different chemical species will be carried out in the future. Further development of the elaboration technique and improvements of the experimental setup are foreseen as well.

In particular, in the near future, the resolution of the spectra (and so the quality of the measurements) is expected to be substantially improved by the installation of a 3600-grooves/mm holographic blazed grating. Moreover, the investigation of the thermochemical properties of the flow in the throat of the nozzle will be carried out using a similar approach.

Acknowledgments

Grateful appreciation for help and advice goes to Antonio Viviani from the Second University of Naples.

References

[1] Park, C. S., Newfield, M. E., Fletcher, D. G., Gökçen, T., and Sharme, S. P., "Spectroscopic Emission Measurement Within Blunt-Body Shock Layer in an Arc Jet Flow," *Journal of Thermophysics and Heat Transfer*, Vol. 12, No. 2, 1998, pp. 190–197. doi:10.2514/2.6344

[2] De Filippis, F., Del Vecchio, A., Viviani, A., Cantiello, I., Natale, M., and Di Costa, M., "Spectroscopic Analysis of Non-Equilibrium Arc Jet in the Plasma Wind Tunnel SCIROCCO," 46th AIAA Aerospace Sciences Meeting and Exhibition, Reno, NV, AIAA Paper 2008-1275, Jan. 2008.

[3] Luque, J., and Crosley, D. R., "LIFBASE (Version 2.0), Database and Spectral Simulation: User Manual," Stanford Research Inst. Rept. MP 99-009, Menlo Park, CA, 1999, pp. 1–21.

[4] Park, C., "Thermochemical Relaxation in Shock Tunnels," *Journal of Thermophysics and Heat Transfer*, Vol. 20, No. 4, Oct.–Dec. 2006, pp. 689–698. doi:10.2514/1.22719

[5] Park, C., "A Review of Reaction Rates in High Temperature Air," AIAA Paper 1989-1740, June 1989.

[6] Millikan, R. C., and White, D. R., "Systematic of Vibrational Relaxation," *Journal of Chemical Physics*, Vol. 39, No. 12, Dec. 1963, pp. 3209–3213. doi:10.1063/1.1734182

[7] Bucchignani, E., and De Filippis, F., "Numerical Simulations of the CIRA PWT SCIROCCO Nozzle for Test Chamber Flow Characterization," *AIDAA XIX National Congress*, Sept. 2007.

[8] De Filippis, F., Schettino, A., Serpico, M., and Borrelli, S., "Complete Analytical Model to Describe the Test-Leg of SCIROCCO PWT," *ICAS 20th Congress*, Sorrento, Italy, Sept. 1996.

[9] Marini, M., De Filippis, F., Del Vecchio, A., Borrelli, S., and Caristia, S., "CIRA 70 MW Plasma Wind Tunnel: a Comparison Between Measured and Computed Exit Nozzle Flow Profiles," *EUROMECH 440 Conference: Aerodynamics and Thermochemistry of High Speed Flow*, Inst. Univ. des Systèmes Thermiques Industriels, Marseilles, France, Sept. 2001.

[10] Anderson, J. D., *Hypersonic and High Temperature Gas Dynamics*, McGraw–Hill International, New York, 2000, Chaps. 10, 11.

[11] Brown, J. M., Colbourn, E. A., Watson, J. K. G., and Wayne, F. D., "An Effective Hamiltonians for Diatomic Molecules: Ab Initio Calculations of Parameters of HCl^+," *Journal of Molecular Spectroscopy*, Vol. 74, No. 2, Feb. 1979, pp. 294–318. doi:10.1016/0022-2852(79)90059-6

[12] Park, C., *Nonequilibrium Hypersonic Aerothermodynamics*, Wiley, New York, 1990, pp. 219–228.

[13] De Filippis, F., "Systematic Previsions of SCIROCCO Performances by Means of CFD Tools," *XIII AIDAA National Congress*, Rome, Sept. 1995.

[14] Borrelli, S., De Filippis, F., Marini, M., and Schettino, A., "CFD for SCIROCCO Project," *Molecular Physics and Hypersonic Flows*, Vol. 482, NATO ASI Series, Kluwer Academic, Norwell, MA, 1996, pp. 302–309.

[15] Caristia, S., De Filippis, F., Del Vecchio, A., and Purpura, C., "SCIROCCO Final Tests Measured Data: Comparison Between Theory and Experiments," *4th European Symposium Aerothemodynamics for Space Vehicles*, Capua, Italy, edited by R. A. Harris, ESA SP 487, 2002, pp. 681–687.

[16] Caristia, S., and De Filippis, F., "Scirocco Project: A Major Plasma Wind Tunnel for the Years 2000," *International Symposium Atmospheric Reentry Vehicles and Systems*, Arcachon, France, 1999.

[17] Marieu, P., Reyner, P., Marraffa, L., Vennemann, D., De Filippis, F., and Caristia, S., "Evaluation of SCIROCCO Plasma Wind-Tunnel Capabilities for Entry Simulations in CO_2 Atmospheres," *Acta Astronautica*, Vol. 61, Nos. 7–8, Oct. 2007, pp. 604–616. doi:10.1016/j.actaastro.2006.12.006

[18] Purpura, C., De Filippis, F., Barrera, P., and Mandanici, D., "Experimental Characterization of the CIRA Plasma Wind Tunnel SCIROCCO Test Section," *Acta Astronautica*, Vol. 62, Nos. 6–7, 2008, pp. 410–421. doi:10.1016/j.actaastro.2008.01.008

[19] De Filippis, F., Del Vecchio, A., Graps, E., and Caristia, S., "Qualification Activities for the SCIROCCO Hypersonic Facility," *Proceedings of the 4th International Symposium Atmospheric Reentry Vehicles and Systems*, Archachon, France, 2005.

[20] *UV-NIKKOR 105 mm f/4.5: Nikon UV Objective Instruction Manual*, Nikon, Tokyo, 2000.

[21] Caristia, S., De Filippis, F., Del Vecchio, A., and Graps, E., "Scirocco PWT facility for high temperature materials, assembly testing," *Proceedings of 54th International Astronautical Congress*, Bremen, Germany, 2003.

[22] De Filippis, F., Purpura, C., Viviani, A., Acampora, L., and Fusco, F., "Spectroscopic Determination of Chemical Species and Non-Equilibrium Temperatures for Air Flows in the SCIROCCO Wind Tunnel," *Journal of Thermophysics and Heat Transfer*, Vol. 24, No. 2, April–June 2010, pp. 271–280. doi:10.2514/1.43050